Pergamon

Int. J. Heat Mass Transfer. Vol. 38, No. 8, pp. 1483–1494, 1995
Copyright © 1995 Elsevier Science Ltd
Printed in Great Britain. All rights reserved
0017-9310/95 $9.50 + 0.00

0017–9310(94)00258–4

Fluid dynamics and condensation-heating of capillary liquid jets

J. MITROVIC and A. RICOEUR

Institut für Technische Thermodynamik und Thermische Verfahrenstechnik, Universität Stuttgart, 70550 Stuttgart, Germany

(*Received* 23 *June* 1994)

Abstract—The subjects of this paper are the hydrodynamics and heating by condensation of a free falling liquid jet. The considerations are based on conservation laws. The equations of continuity, momentum, and energy are integrated numerically, leading to distributions of velocity and temperature in the jet. It is shown that the velocity field in the jet is mainly influenced by the action of gravity. The jet shape obtained numerically depends, among others, on the surface tension and can be well described by a relation derived from a simplified momentum equation. The temperature distribution in the jet is similar to that in developing flows. It depends mainly on Reynolds and Prandtl numbers. On the basis of numerical results, a correlation for the mean jet temperature is recommended. This correlation describes experimental data from the literature satisfactorily.

1. INTRODUCTION

Liquid jets have attracted the attention of natural scientists for centuries. First observations were made on natural jets like waterfalls and geysers. Investigations on artificially produced liquid jets were undertaken, among others, by Venturi [1], Bidone [2] and Savart [3] during the first half of the nineteenth century. At that time, the main interest was focused on the shape and on the break up of liquid jets discharging from orifices of different cross-sections. Major contributions to a tentative finish of such investigations are due to Magnus [4], who published extensive observations on liquid jets of different shapes.

First studies of jet stability were apparently undertaken by Plateau [5], whose principal interest targeted the stability of liquid cylinders with a special regard to surface tension. The effect of gravity hereby was suppressed by producing a cylinder of olive oil within an alcohol–water mixture of equal density. Plateau observed that the oil cylinder becomes instable and breaks up into drops if the length of the cylinder exceeds its circumference.

Theoretical considerations concerning the stability of inertial and viscous liquid jets discharging downward into a vacuum were for the first time presented by Rayleigh. His considerations were later on completed by Bohr and Tomotika so far as the jet environment was also considered as inert and viscous. As far as their results and the results of numerous further publications on jet stability are concerned, the reader may be referred to an extensive review prepared by McCarthy and Molloy [6].

The analytical description of jet shapes using potential flows dates back to Kirchhoff [7]. He neglected external forces and assumed the pressure at the jet surface to be constant. These assumptions led him to analytical equations for the shape of two-dimensional (2D) jets.

Despite numerous investigations on jet dynamics, the flow fields in free falling liquid jets have not been described analytically on the basis of physical models. It is still necessary to integrate hydrodynamic equations numerically, taking into account complex boundary conditions, and (in the case of a comprehensive analysis) the influence of the surface tension. The same also applies to the heating or cooling of liquid jets.

2. THE NATURE OF THE PROBLEM

The motivation for this paper originated in connection with vapour condensation on horizontal tubes, which are arranged in a vertical row. In such a tube arrangement, liquid jets are formed between the tubes within a certain range of parameters. The average temperature of the jet leaving the tube is lower than the saturation temperature. Therefore, vapour condensation takes place not only at the tube but also at the jet surface, decreasing the condensate subcooling. If this subcooling becomes almost completely suppressed, the jet nearly reaches the saturation temperature when reaching the lower tube. In this case, particularly in the upper region of this tube, the heat transfer takes place without or only with a weak vapour condensation. The condensate hereby is cooled and at the circumference of the tube an increasing thermal boundary layer is formed. The condensation starts after the thermal boundary layer has reached the phase interface. These effects influence the condensation process generally and should be con-

NOMENCLATURE

a	thermal diffusivity
d	jet diameter
Fr	Froude number, $u_0^2/(gd_0)$
g	gravitational acceleration
Gz	Graetz number, $Re\ Pr\ d_0/x$
Δh	enthalpy of condensation
J_0	Bessel function
$\dot{M}$	mass flow rate
Nu	Nusselt number, $\alpha d_0/\lambda$
p	pressure
Δp_σ	Laplace pressure
Pr	Prandtl number, ν/a
r	radial coordinate ($\bar{r} = r/r_s$)
r', r''	derivations of r with respect to x
Re	Reynolds number, $u_0 d_0/\nu$
u	velocity of the jet ($\bar{u} = u/u_0$)
v	radial velocity ($\bar{v} = v/u_0$)
We	Weber number, $\sigma/(d_0 u_0^2 \rho)$
x	axial coordinate ($\bar{x} = x/r_0$).

Greek symbols

α	heat transfer coefficient
β_i	roots of the Bessel function
δ	thickness of the condensate film
η	dynamic viscosity
ϑ	temperature
θ	nondimensional temperature
λ	thermal conductivity
ν	kinematic viscosity
ρ	density
σ	surface tension
ψ	contraction number.

Subscripts

m	average
0	initial
s	at phase interface
v	vapour
w	at wall.

sidered for a deeper understanding of heat transfer with vapour condensation on horizontal tubes.

The flow within a condensate jet leaving a horizontal tube is three-dimensional and exposed to complex effects caused by surface tension, particularly in the upper region where the tube is still of considerable influence. A velocity maximum has to be expected at the jet surface as is schematically shown in Fig. 1. At the origin ($x = 0$) of the jet, the velocity of the jet axis is zero. The axial velocity of the jet increases with the vertical distance from the tube so that the velocity profile in the jet cross-section becomes increasingly flat. Similar conditions can also be found for the temperature profile within the jet. In the cross-section at $x = 0$, the jet axis has the wall temperature ϑ_w and the mean temperature of the condensate is lower than the saturation temperature. Due to permanent condensation at the jet surface, the temperature of the condensate increases with increasing jet length.

In fact, the flow and temperature fields in the initial region of the jet are very complex. Therefore, they are simplified in order to allow the investigations, the results of which will be reported in this paper. As shown in Fig. 2, the jet is considered to be of circular cross-section all along the x-axis: further, a constant temperature ϑ_0, and a homogeneous initial velocity u_0 are assumed in its origin ($x = 0$). The liquid jet is surrounded by saturated vapour of temperature

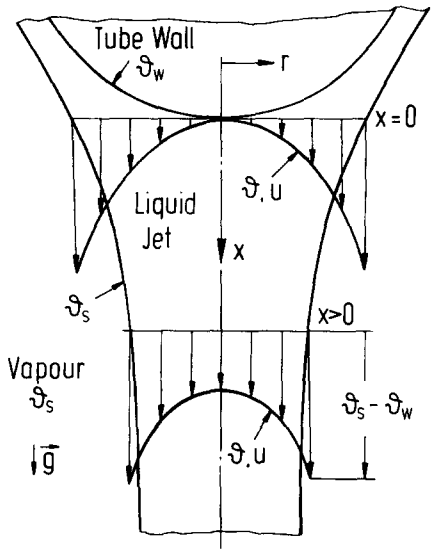

Fig. 1. Schematics of velocity and temperature distributions in a condensate jet leaving a horizontal tube.

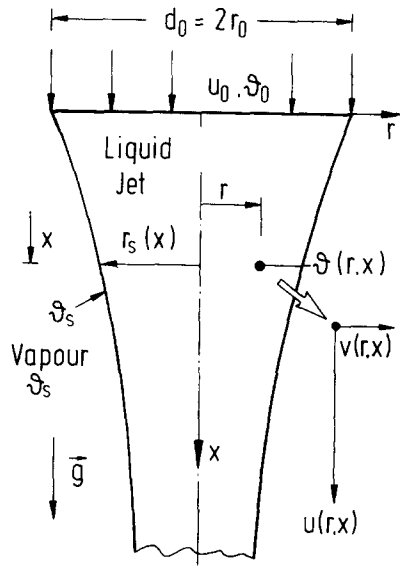

Fig. 2. Physical model.

$\vartheta_s > \vartheta_0$. Vapour and liquid are two phases of the same substance. The jet surface is at saturation temperature and a shear stress is acting at the interface. According to the Eulerian view, the jet flow is steady, axisymmetric, and laminar. The same assumptions are applied to the temperature within the jet.

In this paper, the flow field, the shape of the jet, and the liquid temperature are determined by solving the conservation equations numerically. Besides, the simplified momentum equation is integrated analytically, giving an equation for the jet shape, and a relation for the mean jet temperature, based on numerical results, is recommended.

3. STATE OF THE ART

3.1. *Fluid dynamics and jet shape*

Experimental studies on the jet shape proved that the radius of gravity driven liquid jets issuing from vertical tubes first increases and then decreases [8]. This phenomenon was explained by a redistribution of stresses in the liquid that starts immediately after the jet leaves the tube. Such a behavior of liquid jets could be confirmed by Duda and Vrentas [9] by numerical integration of the governing equations. Additionally, the authors found out that a higher surface tension corresponds to a larger jet radius. In reference to these results, it was concluded that the surface tension causes a resistance to the jet flow.

At nearly the same time, the jet flow was investigated by Lienhard [10]. As did Duda and Vrentas, Lienhard assumed a Poiseuille velocity profile in the initial segment of the jet. However, his numerical calculations were restricted to a range of parameters that justifies the neglect of the surface tension.

Scheuermann [11] seems to be the first to consider the influence of surface tension upon the jet shape. Starting from an energy equation applied to a non-viscous jet, he derived the following relationship between the jet length x and the jet radius r_s:

$$x = \frac{u_0^2}{2g}\left(\left(\frac{r_0}{r_s}\right)^4 - 1\right) + \frac{2\sigma}{r_0 g\rho}\left(\frac{r_0}{r_s} - 1\right). \tag{1}$$

Here g is the gravitational acceleration, σ is the surface tension, and ρ is the liquid density. The meaning of the geometric variables x, r_0 and r_s may be taken from Fig. 2.

If the surface tension σ in equation (1) is set zero, an equation, already noted by Weisbach in 1855, follows:

$$x = \frac{u_0^2}{2g}\left(\left(\frac{r_0}{r_s}\right)^4 - 1\right). \tag{2}$$

For the purpose of a comparison with further equations considered below, equation (1) is written non-dimensionally:

$$\frac{1}{Fr}\frac{x}{r_0} = \left(\frac{1}{\psi^4} + 4We\frac{1}{\psi}\right) - (1 + 4We) \tag{3}$$

by using the Froude number Fr, the contraction number ψ, and the Weber number We given by

$$Fr = \frac{u_0^2}{g d_0}, \tag{4}$$

$$\psi = \frac{r_s}{r_0}, \tag{5}$$

$$We = \frac{\sigma}{d_0 u_0^2 \rho}. \tag{6}$$

Jet equations similar to equation (3) were later recommended by several authors. These equations were summarized in a paper published by Adachi *et al.* [12] and can be written as

$$\frac{1}{Fr}\frac{x}{r_0} = \left(\frac{1}{\psi^4} + nWe\frac{1}{\psi}\right) - (m + nWe). \tag{7}$$

The values of the coefficients m and n are:

$m = 1$, $n = 0$ (Scriven and Pigford, 1959),

$m = 1$, $n = 8$ (Kurabayashi, 1968),

$m = 16/9$, $n = 0$ (Lienhard, 1968),

$m = 1$, $n = 4$ (Anno, 1977).

The coefficients ($m = 1, n = 4$) given by Anno in 1977 and by Scheuermann [11] in 1919 are identical, whereas Scriven and Pigford use the Weisbach equation (2) to determine the local jet radius.

For the jet shape, Adachi *et al.* [12] recommended the equation

$$\frac{1}{Fr}\frac{x}{r_0} = \frac{1}{\psi^4} - m + \left(2We + \left((2We)^2 + \frac{24}{Re\,Fr}\right)^{1/2}\right)\left(\frac{1}{\psi} - n\right), \tag{8}$$

which, contrary to the former equations, contains the Reynolds number Re:

$$Re = \frac{u_0 d_0}{\nu}, \tag{9}$$

and therefore takes into account the liquid viscosity.

The coefficients m and n in equation (8) were determined from experiments. It is to be noted that equation (8) becomes identical to equation (3), if the Reynolds number assumes very large values ($Re \to \infty$).

3.2. *Heat transfer*

The heating of liquid jets was the subject of several investigations [13–30]. Kutateladze [13] seems to be the first to deal with this problem theoretically. He assumed the jet velocity to be invariable with respect to the radial position and used equation (2) to calculate the jet radius. By making some further simplifications, Kutateladze solved the energy equation by separating the variables and obtained the average

temperature ϑ_m in a jet cross-section in the case of a laminar flow as

$$\frac{\vartheta_s-\vartheta_m}{\vartheta_s-\vartheta_0}=\sum_{i=1}^{6}\frac{4}{\beta_i^2}\exp\left(-\beta_i^2\frac{4}{Re\,Pr}\frac{x}{d_0}\right)+S \quad (10)$$

where β_i are roots of the Bessel functions $J_0(\beta_i)=0$, Re is the Reynolds number given by equation (9), Pr is the Prandtl number and S is the sum of the residual terms of the infinite series. The ratio x/d_0 represents the jet length divided by the initial jet diameter, ϑ_0 is the initial temperature ($x=0$) and ϑ_s is the temperature of the jet surface.

For the sum S, Isachenko *et al.* [18] proposed the relation

$$S=\frac{4}{\pi}\frac{1}{\beta_7}\exp\left(-\beta_7^2\frac{4}{Re\,Pr}\frac{x}{d_0}\right)-\frac{4}{\sqrt{\pi}}\left(\frac{4}{Re\,Pr}\frac{x}{d_0}\right)^{1/2}\operatorname{erfc}\left(\beta_7\left(\frac{4}{Re\,Pr}\frac{x}{d_0}\right)^{1/2}\right)+\frac{2}{\beta_7^2}\exp\left(-\beta_7^2\frac{4}{Re\,Pr}\frac{x}{d_0}\right), \quad (11)$$

which contains the complementary error function $\operatorname{erfc}(x)=1-\operatorname{erf}(x)$. The error function can be calculated by [31]

$$\operatorname{erf}(x)\approx\sqrt{1-\exp(-1{,}26x^2)}, \quad (12)$$

if an engineering accuracy is required.

In connection with the question raised by Dementyeva and Makarov [24] concerning the convective part of the heat flux towards the jet axis in Kutateladze's considerations, the results of Kutateladze [13] have been recently discussed by Hoang and Seban [25].

Hasson *et al.* [17] investigated the heating of the jet in a similar way to Kutateladze and they suggested an equation for the average jet temperature which corresponds to equation (10). Parts of these considerations were recently reviewed by Celata *et al.* [28]. An analysis presented by Jacobs and Nadig [30] allowed the derivation of an equation for the heat transfer which corresponds to the usual penetration relations.

In some publications, the jet heating is examined by simultaneous numerical integration of differential equations. Murty and Sastry [20] assumed distributions for velocity and temperature in the jet cross-section, a fact which significantly restricts the results obtained. Mochalova *et al.* [21, 23] treated the equations of conservation in differential form numerically. Besides the Reynolds and the Prandtl number, these authors include the Weber number in their considerations, and therefore the influence of the surface tension on the heat transfer in the jet.

In most cases, experimental research concerning jet heating due to vapour condensation was carried out on liquid jets issuing out of tubes [15–19, 24, 27, 28]. In these cases, especially near the orifice of the tube, heat transfer conditions are significantly different compared with those prevailing on jets formed by condensation on horizontal tubes. At present, a paper by Kutateladze *et al.* [26] seems to be the only one which deals with the heating of condensate jets formed between horizontal tubes. The results presented in their paper show a considerably stronger decrease of the condensate subcooling compared with the heating of a jet discharged from an orifice.

4. PHYSICAL MODEL AND MATHEMATICAL FORMULATION

Heat transfer in a laminar, axisymmetric, and steady jet flow, as shown in Fig. 2, is described by the following equations:

the equation of continuity:

$$\frac{\partial}{\partial r}(rv)+\frac{\partial}{\partial x}(ru)=0 \quad (13)$$

the equations of momentum in radial and axial directions:

$$v\frac{\partial v}{\partial r}+u\frac{\partial v}{\partial x}=-\frac{1}{\rho}\frac{\partial p}{\partial r}+\nu\left(\frac{\partial^2 v}{\partial r^2}+\frac{1}{r}\frac{\partial v}{\partial r}-\frac{v}{r^2}+\frac{\partial^2 v}{\partial x^2}\right) \quad (14)$$

$$v\frac{\partial u}{\partial r}+u\frac{\partial u}{\partial x}=-\frac{1}{\rho}\frac{\partial p}{\partial x}+g+\nu\left(\frac{\partial^2 u}{\partial r^2}+\frac{1}{r}\frac{\partial u}{\partial r}+\frac{\partial^2 u}{\partial x^2}\right) \quad (15)$$

and the equation of energy:

$$v\frac{\partial\vartheta}{\partial r}+u\frac{\partial\vartheta}{\partial x}=a\left(\frac{\partial^2\vartheta}{\partial r^2}+\frac{1}{r}\frac{\partial\vartheta}{\partial r}+\frac{\partial^2\vartheta}{\partial x^2}\right). \quad (16)$$

In these equations, v and u denote the radial and the axial velocity components, p the pressure, g the gravitational acceleration, ρ the density, ν the kinematic viscosity, ϑ the temperature, and a the thermal diffusivity of the jet liquid.

4.1. *Simplifications and boundary conditions*

For the sake of simplicity, the terms in equation (14) are considered to be small compared with those in equation (15). Therefore, equation (14) can be omitted. If the derivation $\partial^2 u/\partial x^2$ in equation (15) is omitted too, equations (13) and (15) simplify to the well-known boundary layer equations. Finally, the system of equations (13) and (15), each applied to both liquid and vapour phase, and equation (16) have to be solved.

The boundary conditions are enunciated as follows:

Jet origin:

$$x=0,\ 0\leqslant r\leqslant r_0:\quad u=u_0,\ v=0,\ \vartheta=\vartheta_0$$

Jet axis:

$$r = 0, x \geqslant 0: \quad \frac{\partial u}{\partial r} = 0, \frac{\partial v}{\partial r} = 0, v = 0, \frac{\partial \vartheta}{\partial r} = 0$$

Jet surface:

$$r = r_s, x \geqslant 0: \quad \vartheta = \vartheta_s, \eta\,|\partial u_s/\partial r| = \eta_v\,|\partial u_v/\partial r|$$

$$p = p_v + \Delta p$$

Condensing steam:

$$x = 0, r > r_0: \quad u_v = u_{v0}, v_v = 0$$

$$x > 0, r \to \infty: \quad u_v = v_v = 0.$$

The conditions on the jet surface allow a pressure jump Δp over the interface from vapour to liquid. This pressure jump can be obtained from a radial momentum balance on an element of the jet surface, the radial velocity of which being neglected, as

$$\Delta p = p - p_v = \Delta p_\sigma + \rho_v v_v^2. \tag{17}$$

In equation (17), Δp_σ is the Laplace pressure, ρ_v is the density and v_v is the velocity of the vapour near the jet surface.

The velocity v_v of the vapour can be obtained by means of an enthalpy balance at the phase interface as

$$v_v = -\frac{\lambda}{\rho_v \Delta h}\left(\frac{\partial \vartheta}{\partial r}\right)_s, \tag{18}$$

where Δh is the enthalpy of condensation, λ is the thermal conductivity, and $(\partial\vartheta/\partial r)_s$ denotes the liquid side temperature derivation at the interface.

The Laplace pressure Δp_σ is given by

$$\Delta p_\sigma = 2\frac{\sigma}{r_m} = \sigma\left(\frac{1}{r_2} - \frac{1}{r_1}\right), \tag{19}$$

where r_2 and r_1 are the main radii of curvature of the jet surface. The following applies in accordance with Fig. 3 for the radii r_1 and r_2:

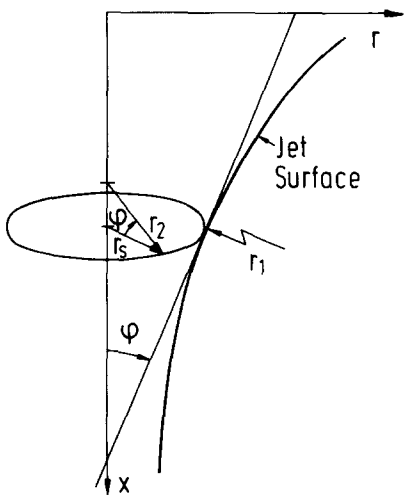

Fig. 3. Main radii of jet curvature.

$$\frac{1}{r_1} = \frac{\dfrac{d^2 r_s}{dx^2}}{\left(1 + \left(\dfrac{dr_s}{dx}\right)^2\right)^{3/2}} = \frac{r_s''}{(1 + r_s'^2)^{3/2}} \tag{20}$$

and

$$\frac{1}{r_2} = \frac{\cos\varphi}{r_s} = \frac{1}{r_s\left(1 + \left(\dfrac{dr_s}{dx}\right)^2\right)^{1/2}} = \frac{1}{r_s(1 + r_s'^2)^{1/2}}. \tag{21}$$

Considering these relations, equation (19) can be written as

$$\Delta p_\sigma = \frac{\sigma}{r_s(1 + r_s'^2)^{1/2}}\left(1 - \frac{r_s r_s''}{1 + r_s'^2}\right). \tag{22}$$

From equations (17), (18) and (22), the liquid side pressure p becomes

$$p = p_v + \Delta p = p_v + \frac{\sigma}{r_s(1 + r_s'^2)^{1/2}}\left(1 - \frac{r_s r_s''}{1 + r_s'^2}\right) + \frac{\lambda^2}{\rho_v \Delta h^2}\left(\frac{\partial \vartheta}{\partial r}\right)_s^2. \tag{23}$$

The pressure p_v in the vapour changes along the jet due to vapour flow and gravitational acceleration g.

4.2. *Numerical procedures*

The system of differential equations (13), (15) and (16) was solved numerically using a finite difference scheme. A grid was applied with a radial distance between the node points of 3×10^{-5} m and an axial distance of 6×10^{-5} m. The algebraic formulation of the differential equations is similar to that described by Marsal [32] for the calculation of laminar boundary layers. The result is a set of linear algebraic equations to be solved at each axial step. However, near $x = 0$, a non-linear algebraic set of equations had to be solved iteratively.

In order to simplify equation (23) and, consequently, the momentum equation (15), the curvature radius r_1 was assumed to be much larger than the jet radius r_s, the pressure at the jet surface due to radial vapour flow was neglected, and the physical properties were regarded as constant.

The uncertainty in the derivations due to discretization in the worst case is proportional to the product between the second derivation of the axial velocity u with respect to x and the axial grid width. The maximum error occurs at the origin of the jet, since the algebraic equations downstream exclusively contain terms of higher accuracy. The numerical error for example in the derivation $\partial u/\partial x$ in the case of $d_0 = 3$ mm and $u_0 = 0.2\text{m s}^{-1}$ does not exceed 0.4% at the jet origin. Because the numerical algorithm is stable, this initial error is smoothed downstream.

In numerical processing of the hydrodynamic equa-

tions calculating the velocity distributions and the jet shape, the influence of the condensation at the jet surface on the flow field was disregarded. To calculate the local velocities at one axial step, the contraction of the jet cross-section was determined by extrapolation from the values obtained upstream. Thus the algebraic set of equations yielded the axial and the radial velocities u and v in one cross-section. The radius of each axial step was subsequently determined using the mean axial velocity and the integral type equation of continuity.

Following the calculation of the velocity profile and the jet shape, the energy equation is solved similarly. The temperature gradient at the phase interface is used to calculate the thickness of the condensate layer along the jet.

5. RESULTS

5.1. *Analytical approach to the jet shape*

Before the results of the numerical integration are presented and discussed, an analytical approach to the jet shape will be undertaken. Herein the following assumptions should be valid: all quantities are invariable with respect to radius; the liquid jet is isothermal; the axial pressure gradient in the vapour is caused by gravity only and there is no interfacial shear stress.

According to these assumptions, the pressure given by equation (23) can be considered to be constant over the jet cross-section. Substituting $p_v = p_{v0} + \rho_v g x$ with constant pressure p_{v0} at $x = 0$ in equation (23) leads to the following relation for the pressure gradient $\mathrm{d}p/\mathrm{d}x$ in the liquid jet:

$$\frac{\mathrm{d}p}{\mathrm{d}x} = \rho_v g + \frac{\mathrm{d}}{\mathrm{d}x}\left(\frac{\sigma}{r_s(1+r_s'^2)^{1/2}}\left(1 - \frac{r_s r_s''}{1+r_s'^2}\right)\right). \tag{24}$$

The above assumptions allow an integration of the momentum equation (15) along the jet axis. Regarding equation (24), the solution reads

$$\frac{u^2}{2} + \frac{\sigma}{\rho r_s(1+r_s'^2)^{1/2}}\left(1 - \frac{r_s r_s''}{1+r_s'^2}\right) + v\frac{\mathrm{d}u}{\mathrm{d}x} = \frac{\Delta\rho}{\rho} g x + C. \tag{25}$$

In this equation, u denotes the average velocity in a jet cross-section at the distance x from the jet origin and can be calculated from the equation of continuity,

$$r_s^2 u = r_0^2 u_0 \tag{26}$$

where r_s is the local jet radius (see Fig. 2).

For further considerations it is convenient to convert equations (25) and (26) into a non-dimensional form using the radius r_0 and the velocity u_0 as characteristic properties.

With

$$\left.\begin{aligned} u &= \bar{u}u_0 \\ r_s &= \psi r_0 \\ x &= \bar{x} r_0 \end{aligned}\right\}, \tag{27}$$

equation (26) yields

$$\psi^2 \bar{u} = 1. \tag{28}$$

Equation (25) can now be expressed as

$$\frac{1}{\psi^4} + \frac{4We}{\psi(1+\psi'^2)^{1/2}}\left(1 - \frac{\psi\psi''}{1+\psi'^2}\right) + \frac{8}{Re}\frac{\psi'}{\psi^3} = \frac{1}{Fr}\frac{\Delta\rho}{\rho}\bar{x} + C. \tag{29}$$

In this equation, We, Re, Fr and ψ are the Weber, the Reynolds, the Froude and the contraction number according to equations (4)–(6) and (9), respectively.

A further analytical integration of equation (29) seems to be impossible. In order to arrive at a relation for the jet radius as a first approximation we assume $\psi' \ll 1$, $\psi'' \approx 0$, and Re large enough so that the term containing the Reynolds number can be neglected. In this case, the integration constant C can be determined from equation (29) using the condition $\bar{x} = 0$, $\psi = 1$ as

$$C = 1 + 4We. \tag{30}$$

Finally, equation (29) takes the approximate form

$$\frac{1}{\psi^4} + \frac{4We}{\psi} - (1 + 4We) = \frac{1}{Fr}\frac{\Delta\rho}{\rho}\bar{x}. \tag{31}$$

This equation allows the calculation of the jet radius ($\psi = r_s/r_0$) as a function of the axial position ($\bar{x} = x/r_0$) if the Weber and Froude numbers are considered as parameters. With $\Delta\rho = \rho$, equation (31) coincides with equation (3) derived by Scheuermann [11] on the base of an energy balance.

5.2. *Numerical results*

5.2.1. *Jet shape and velocity profiles.* Figure 4 shows the shape of a 200 mm long water jet obtained by numerical integration of equations (13) and (15). The initial ($x = 0$) jet diameter is 2 mm, and an initial jet velocity of 0.3 m s^{-1} was chosen. The physical properties were taken at the saturation temperature.

As follows from this figure, a significant contraction of the jet cross-section takes place in the upper region of the jet. Within the first 50 mm the jet diameter decreases to nearly half of its initial value. This implies a small convex curvature radius r_1 in Fig. 3 so that the simplification $r_1 \to \infty$ made above could lead to considerable errors in the numerical solution. For thin jets with a large initial velocity, as in the above example, the error does not exceed a few percent because the contribution of r_1 to the capillary pressure is small in comparison to the contribution of r_2. As far as jets with larger initial diameters and smaller initial velocities are considered, a stronger jet contraction is expected which can change the sign of capillary

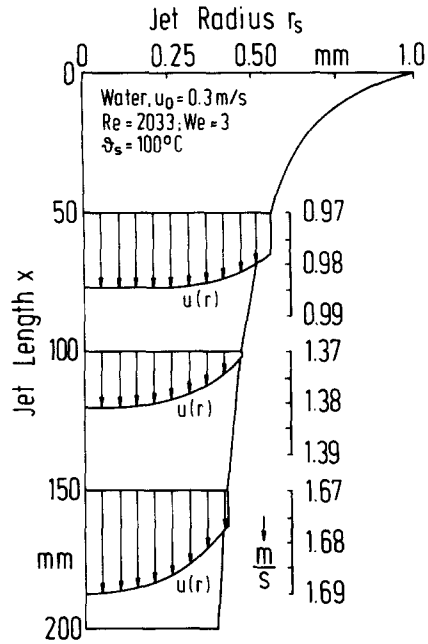

Fig. 4. Jet shape and distribution of axial velocity in a water jet.

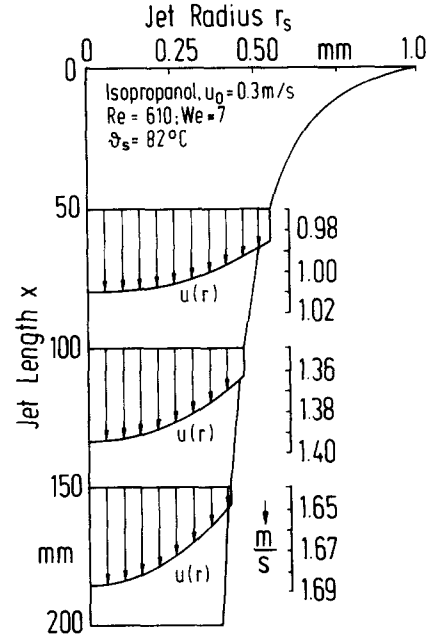

Fig. 5. Jet shape and distribution of axial velocity in an isopropanol jet.

pressure in the upper region of the jet. This happens for example with a water jet of $r_0 = 2$ mm and $u_0 = 0.1$ m s^{-1}. However, this effect remains restricted to a small jet length because, already, at $x = 5$ mm the difference between the average curvature radius r_m and the local jet radius r_s hardly exceeds a few percent.

Figure 4 also shows the profiles of the axial velocity u in cross-sections at $x = 50$ mm, 100 mm and 150 mm. On the right-hand side of the figure, the velocity values u in m s^{-1} are indicated. The decrease of the velocity towards the jet surface is due to the interfacial shear stress, which increases with x. The absolute values of the velocity, however, are essentially dominated by gravity.

According to numerical results in this paper, the radial velocity v decreases from the maximum value at the interface almost linearly towards zero on approaching the jet axis. Such a distribution of the radial velocity also follows from the equation of continuity (13), if the derivation $\partial u/\partial x$ is taken to be invariable with respect to radius. Compared to the axial velocity, the absolute values of the radial velocity are negligible.

As shown in Fig. 5, the shape of an isopropanol jet is similar to that of a water jet. However, the profiles of the axial velocities are more pronounced for alcohol than for water. This can be explained by the differences in viscosity, which is 2.5 times larger for alcohol than for water in the liquid phase, and about 7.5 times larger in the vapour phase.

Figure 6 compares the jet shapes obtained numerically with those calculated analytically according to equation (31). Shown in this figure is the difference $(r_s/r_{sid} - 1)$, where r_{sid} is the jet radius according to equation (2), vs the non-dimensional jet length $\Delta\rho x/(Fr\,\rho r_0)$. The solid lines represent the numerical, the dashed ones the analytical results according to equation (31). As can be seen from the figure, there is hardly a considerable deviation between the numerical and the analytical values using equation (2). The largest deviation appears in the region with significant changes in the local jet radius and hence can be attributed to the action of the surface tension σ on the mean jet velocity. Assuming a decreasing jet radius, a

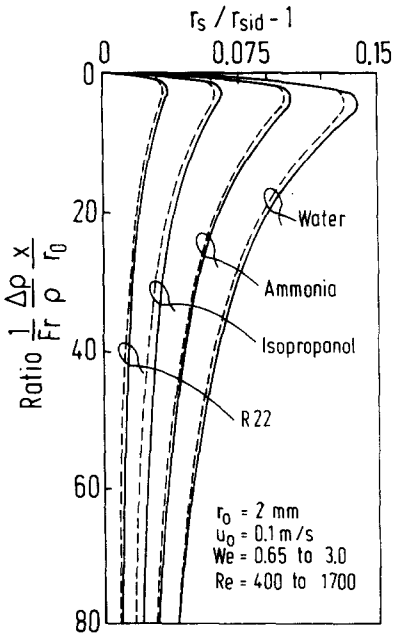

Fig. 6. Comparison of numerically obtained jet radii with equation (31). Solid lines: numerical values, dashed lines: equation (31).

larger surface tension leads to a higher flow resistance. Thus, the jet radius increases if the mass flow rate within the jet is taken to be constant. Moreover, the figure indicates a satisfactory agreement between numerical and analytical solutions within the entire range of parameters.

The results shown in Fig. 6 are obtained with different substances at equal initial values u_0 and r_0. Lower values of u_0 and r_0 lead to higher deviations of the actual jet shape from that according to equation (2). This is caused by an increased curvature of the phase interface for lower values of u_0 and r_0, leading to an increase in resistive action of the surface tension and subsequently to a lower mean jet velocity.

The analytical considerations and the numerical calculations allow the conclusion that, within the scope of the simplifications made, the jet shape can be well determined by the analytical equation (31). Since this equation does not take into account the influence of viscosity, its validity is restricted to liquids of low viscosity. The axial jet velocity is essentially determined by gravity. Along the jet surface, this velocity is mainly affected by the interfacial shear stress.

5.2.2. *Heating of the jet.* Figure 7 shows radial temperature profiles in a water jet with a mass flow rate $\dot{M}$ of 0.5 g s^{-1} taken at several distances x from the jet origin. In this figure, the non-dimensional temperature θ given by

$$\theta = \frac{\vartheta - \vartheta_0}{\vartheta_s - \vartheta_0} \tag{32}$$

is plotted vs the non-dimensional jet radius $\bar{r} = r/r_s$. The parameters used to perform the calculations can be taken from Fig. 7. As shown in this figure, a decrease in the temperature gradient at the interface ($r/r_s = 1$) as well as an increase in the jet heating with the jet length is observed. At approximately $x = 50$ mm, the temperature at the jet axis starts to rise. The subcooling of the liquid in the jet axis decreases by about a half at $x = 200$ mm. Radial temperature profiles similar to those in Fig. 7 were also obtained for jets of other liquids.

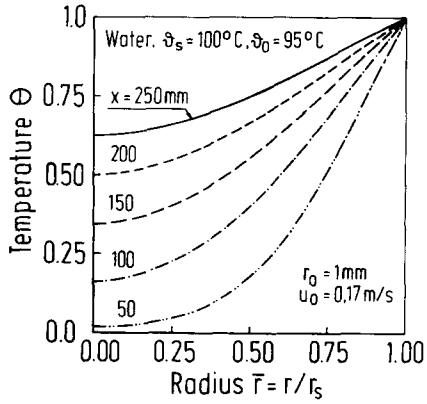

Fig. 7. Temperature distribution in some jet cross-sections.

Figure 8 shows the mean temperature θ_m over a cross-section vs the jet length x for several mass flow rates. The calculations were based on physical properties taken at the saturation temperature: the initial subcooling is 5 K in each case. As indicated in the figure, only the jet with the lowest mass flow rate $\dot{M} = 0.15$ g s^{-1} attains the saturation temperature all over the cross-section at a length of approximately 250 mm.

As a further example, the mean temperatures of isopropanol jets are given in Fig. 9. In this case, the increase in temperature is significantly lower compared to that of a water jet. This is essentially due to the lower thermal conductivity of isopropanol.

In order to illustrate the effect of physical properties on the jet heating, the calculated mean temperature θ_m of jets of several liquids is plotted in Fig. 10. The initial subcooling and the mass flow rate are the same for all liquids. All calculations are carried out with the physical properties at saturation. As can be seen, isopropanol shows a distinctly lower heating compared to other substances. This is mainly due to the low thermal diffusivity of alcohol. However, this parameter is certainly not the only one which is decisive for the jet heating. The thermal diffusivity of water, for example, is about 17% lower compared to that of ammonia: nevertheless, the heating of water is stronger. Obviously, more detailed considerations of this subject must take into account further physical properties as, for example, the liquid density. This parameter decisively determines the mean jet velocity, and thus the local jet radius, and, consequently, the jet heating.

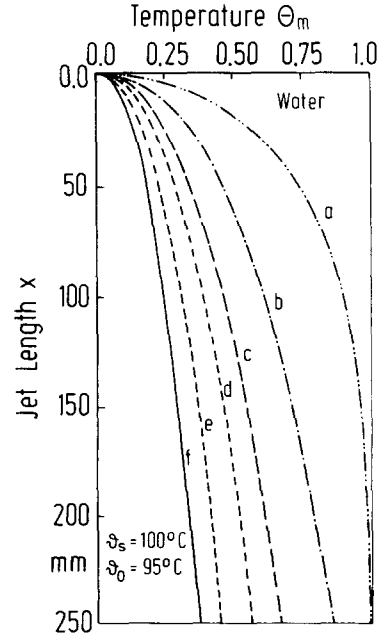

Fig. 8. Mean temperature of water jets as a function of jet length for different mass flows. (a) $\dot{M} = 0.15$ g s^{-1}, (b) $\dot{M} = 0.5$ g s^{-1}, (c) $\dot{M} = 1.0$ g s^{-1}, (d) $\dot{M} = 1.5$ g s^{-1}, (e) $\dot{M} = 2.5$ g s^{-1}, (f) $\dot{M} = 4.0$ g s^{-1}.

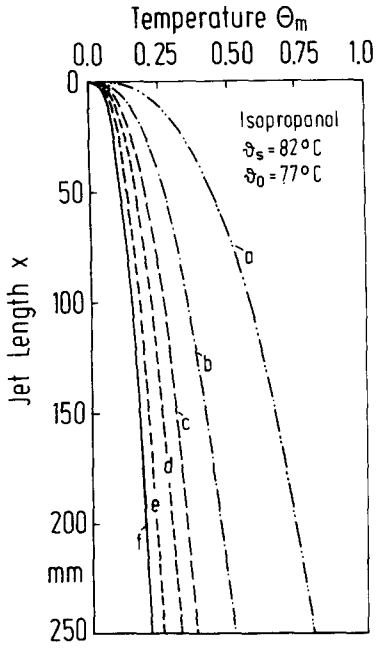

Fig. 9. Mean temperature of isopropanol jets as a function of jet length for different mass flows. (a) $\dot{M} = 0.15$ g s^{-1}, (b) $\dot{M} = 0.5$ g s^{-1}, (c) $\dot{M} = 1.0$ g s^{-1}, (d) $\dot{M} = 1.5$ g s^{-1}, (e) $\dot{M} = 2.5$ g s^{-1}, (f) $\dot{M} = 4.0$ g s^{-1}.

The numerical results of this paper confirm the facts observed by other authors, namely, the perception that the initial subcooling is only of minor influence on the mean normalized jet temperature θ_m. Moreover, the heating of the liquid depends strongly on the mass flow rate, as expected. Here it is irrelevant, whether the mass flow rate is changed by varying the initial radius r_0 or the initial velocity u_0.

The presented results concerning the jet heating are based on the assumptions that the jet shape is not affected by vapour condensation, and that the thickness of the condensate film at the jet surface is negligible compared with the jet radius. As Fig. 11 illustrates, this assumption is permissible. The figure shows, as an example, the thickness of the condensate film on a water jet. It can be seen that the condensate film is hardly thicker than 1.5% of the initial jet radius, although an initial subcooling of 60 K and a jet length of 250 mm were assumed. In condensation on tube bundles, under realistic conditions, the subcooling as well as the jet length are considerably smaller. Therefore, the condensate added to the jet is supposed to have a minor influence on the jet shape and the liquid side heat transfer.

6. CORRELATIONS

With regard to a practical application of the numerical results obtained, it is useful to develop a suitable correlation for the jet heating. In order to derive such a correlation, it is convenient to convert the energy equation into a non-dimensional form.

If the temperature ϑ of the jet is replaced by θ according to equation (32) and considering the expressions (27), equation (16) can be written as

$$\bar{v}\frac{\partial\theta}{\partial\bar{r}}\frac{1}{\psi}+\bar{u}\frac{\partial\theta}{\partial\bar{x}}=\frac{2}{Re\,Pr}\left(\frac{1}{\psi^2}\frac{\partial^2\theta}{\partial\bar{r}^2}+\frac{1}{\psi^2}\frac{1}{\bar{r}}\frac{\partial\theta}{\partial\bar{r}}+\frac{\partial^2\theta}{\partial\bar{x}^2}\right). \tag{33}$$

According to this equation, the jet heating, besides

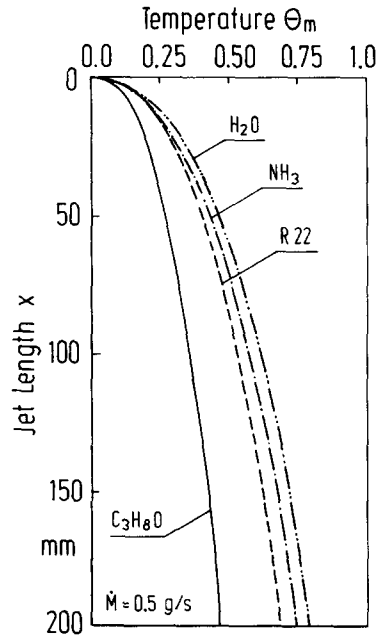

Fig. 10. Mean temperature of jets of different liquids depending on jet length.

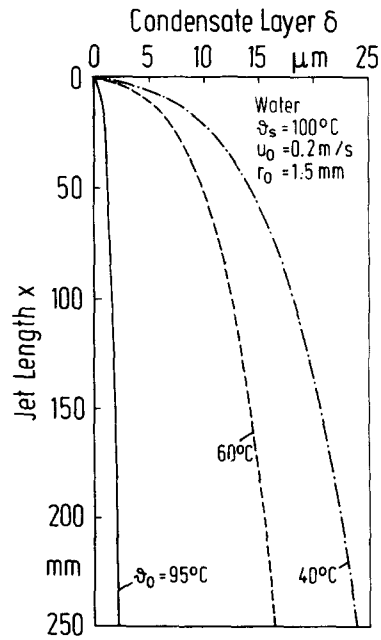

Fig. 11. Thickness of condensate layer on water jets.

the Reynolds and the Prandtl number, depends on the contraction number ψ and hence on the parameters controlling the hydrodynamics of the jet, namely, the Weber and the Froude numbers, see equation (31).

Although ψ is a function of *Re*, *Fr* and *We* all calculated values of the mean non-dimensional temperature θ_m become almost identical if the product $Re\,Pr\,x/d_0$ is used as a variable. In this case, the values of the temperature θ_m scatter less than 2% for all liquids at all conditions chosen for calculations.

For the practical purpose, the numerical values of the mean jet temperature θ_m can be quite well described by

$$\theta_m = \frac{\vartheta_m - \vartheta_0}{\vartheta_s - \vartheta_0} = 1 - \exp\left(-4.8\left(\frac{4}{Re\,Pr}\frac{x}{d_0}\right)^{0.7}\right). \quad (34)$$

Considering the logarithmic mean temperature difference and assuming a constant jet diameter $d = d_0$, a heat balance for the jet section between $x = 0$ and x yields

$$Nu_m \equiv \frac{\alpha_m d_0}{\lambda} = \frac{Re\,Pr}{4}\frac{d_0}{x}\ln\frac{1}{1-\theta_m}. \quad (35)$$

Inserting θ_m according to equation (34) in equation (35) results in

$$Nu_m = 4.8\left(\frac{Re\,Pr}{4}\frac{d_0}{x}\right)^{0.3}. \quad (36)$$

This equation implies that the mean Nusselt number Nu_m and hence the mean heat transfer coefficient α_m decreases as the jet length x increases. Equation (38) coincides principally with the Lévêque [33] equation for laminar flows.

7. COMPARISON WITH PREVIOUS STUDIES

Figure 12 compares the jet heating according to equations (10) and (34). Herein, the mean temperature θ_m is plotted vs the non-dimensional jet length $(4/Re\,Pr)(x/d_0)$. For low values of this parameter (0.01–0.04), equation (34) shows lower values of θ_m. This could be due to the effect of the surface tension which reduces the jet velocity.

Figure 13 shows a comparison of the experimental values of Lui *et al.* [34] with equation (34). In this figure, the mean temperature θ_m is plotted vs the Graetz number $Gz = Re\,Pr\,d_0/x$. The experiments were carried out with water jets at different initial subcoolings (different Jakob numbers). The measurements indicate, in agreement with the numerical results, that the jet heating is only casually affected by the Jakob number. Figure 13 shows further that the experimental results are below the numerical curve. This is partly due to the manner of jet formation. Measurements carried out by several authors proved that the jet heating also depends on the conditions of jet formation. However, the significant deviation between experimental and calculated values in this case can be explained by the presence of air in the condensing vapour. As Lui *et al.* [34] pointed out, the percentage of air in the vapour amounted to up to 0.4%.

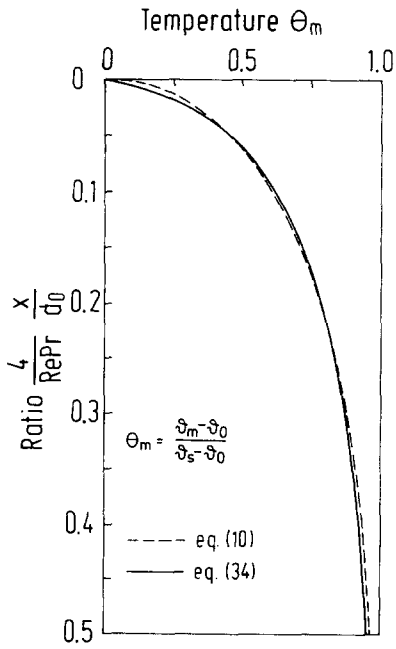

Fig. 12. Comparison of Kutateladze equation (10) with equation (34).

Fig. 14 compares measurements by Celata *et al.* [28] with numerical values of this paper. Herein, the normalized temperature θ_m is plotted vs the length x for mass flow rates $\dot{M}$ of 1.67, 3.33 and 6.67 g s^{-1}. The curves presented are calculated according to equation (34). As Fig. 14 shows, the agreement is satisfactory for low values of x, while there is a distinct deviation of the experimental data towards higher values. The strong rise in the experimental data between $x = 70$ mm and $x = 120$ mm is particularly striking. This could be caused by the formation of axisymmetrical waves and jet vibrations that are frequently observed at larger jet lengths. Moreover, a sudden acceleration of the jet surface is expected after the liquid left the

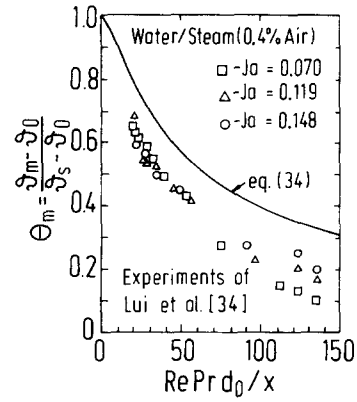

Fig. 13. Comparison of experimental results of Lui *et al.* [34] with equation (34).

nozzle, causing a vortex formation near the phase interface, and an increase in heat transfer.

8. SUMMARY AND CONCLUSIONS

In this paper, the flow and the heating of viscous liquid jets discharged vertically into a region of their own vapour were examined numerically. The investigations were based upon the laws of conservation in differential form, taking into account the surface tension as well as the interfacial shear stress. Boundary conditions were, among others, a flat velocity and temperature profile in the initial segment of the jet. The effect of condensation on the jet shape was investigated and proved to be negligible.

Concerning the jet shape, it could be shown, that the effect of the surface tension should not be neglected, particularly for jets at low initial velocities, whereas the effect of the interfacial shear stress is of minor significance in most cases. Furthermore, equation (1) derived by Scheuermann, which can also be derived from an analytical solution of the simplified momentum equation, agrees well with the numerical data of this paper.

The mean jet temperature in a cross-section attains saturation temperature only for large jet lengths and low mass flow rates. The numerically determined jet temperatures can be approximated by a simple correlation. Based upon this correlation, an equation for the mean heat transfer coefficient is recommended.

The results obtained for the jet heating are compared with the analytical solution of the energy equation given by Kutateladze [13], who assumed a jet shape according to equation (2) and a constant velocity in the jet cross-section. Particularly in the range of long jets, a good agreement is achieved. Furthermore, the numerical results are also compared with measurements taken from literature. The experimental data of Lui *et al.* [34] differ from the theoretical values because of the presence of non-condensibles in the condensing vapour. In a range of small jet lengths, the measurements of Celata *et al.* [28] agree well with our correlation.

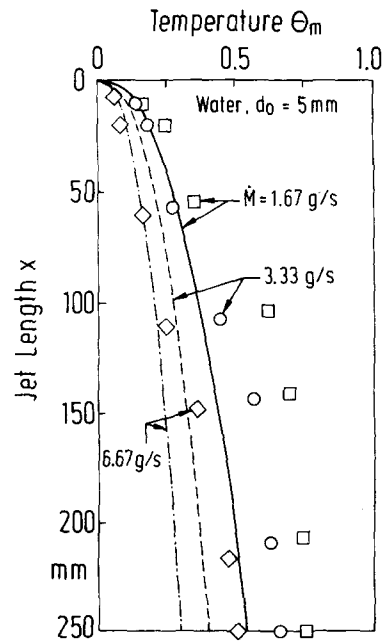

Fig. 14. Comparison of experimental results of Celata *et al.* [28] with equation (34).

Acknowledgements—The authors wish to express their gratitude to Mrs M. Franz and Prof. K. Stephan for many fruitful discussions and valuable suggestions.

REFERENCES

1. J. B. Venturi, Untersuchungen und Erfahrungen über die Seitenmitteilung der Bewegung in flüssigen Körpern, angewandt auf die Erklärung verschiedener hydrodynamischer Erscheinungen, *Gilberts Annln Phys.* **3** 129–166 (1800).
2. G. Bidone, *Expériences sur la forme et sur la direction des veines et des courants d'eau lancés par diverses ouvertures.* S. 1–136. Imprimerie Royale, Turin (1829).
3. F. Savart, Über die Beschaffenheit der durch kreisrunde Öffnungen aus dünner Wand strömenden Flüssigkeitsstrahlen, *Annln Phys. Chem.* **109,** 451–477 (1834).
4. G. Magnus, Über die Bewegung der Flüssigkeiten, *Annln Phys. Chem.* **156,** 1–36 (1850); Hydrodynamische Untersuchungen, *Annln Phys. Chem.* **171,** 1–59 (1855) und **192,** 1–32 (1859).
5. J. Plateau, Experimentelle und theoretische Untersuchungen über die Gleichgewichtsfiguren einer flüssigen Masse ohne Schwere, *Annln Phys. Chem.* **158,** 387–405 (1851).
6. M. J. McCarthy and N. A. Molloy, Review of stability of liquid jets and the influence of nozzle design, *Chem. Engng J.* **7,** 1–20 (1974).
7. G. Kirchhoff, *Vorlesungen über Mathematische Physik*, Bd. I: Mechanik, 4. Auflage, Leipzig (1897).
8. S. Middleman and J. Gavis, Expansion and contraction of capillary jets of Newtonian liquids, *Phys. Fluids* **4,** 355–359 (1961).
9. J. L. Duda and J. S. Ventras, Fluid mechanics of laminar liquid jets, *Chem. Engng Sci.* **22,** 855–869 (1967).
10. J. H. Lienhard, Effects of gravity and surface tension upon liquid jets leaving Poiseuille tubes, *Trans. ASME J. Basic Engng* **90,** 262–268 (1968).
11. R. Scheuermann, Über die Gestalt und die Auflösung des fallenden Flüssigkeitsstrahles, *Annln Phys.* IV. Folge **60,** 233–259 (1919).
12. K. Adachi, K. Tagashiva, Y. Banba, H. Tatsumi, H. Machida and N. Yoshioka, Steady laminar round jets of a viscous liquid falling vertically in the atmosphere, *A.I.Ch.E. Jl* **36,** 738–745 (1990).
13. S. S. Kutateladze, *Heat Transfer with Condensation and Boiling.* Mashgiz (1952) [in Russian]
14. M. P. Poljak, Heating of falling liquid jet in cross-flow of vapour *J. Engng Phys.* **4**(6), 119–121 (1961).
15. J. R. Maa, Condensation of vapor on a very cold liquid stream, *Ind. Engng Chem. Fundam.* **8,** 560–563 (1969).
16. J. R. Maa, Condensation studies with the jet steam tensimeter, *Ind. Engng Chem. Fundam.* **8,** 564–570 (1969).
17. D. Hasson, D. Luss and R. Peck, Theoretical analysis of vapor condensation on laminar liquid jets, *Int. J. Heat Mass Transfer* **7,** 969–981 (1964).
18. V. P. Isachenko, A. P. Solodov, Yu. Z. Samoilovich, V. I. Kushnyrev and S. A. Sotskov, Investigation of heat transfer with steam condensation on turbulent liquid jets, *Thermal Engng* **18**(2), 8–12 (1971).
19. V. P. Isachenko and A. P. Solodov, Heat transfer with

steam condensation on continuous and dispersed jets of liquid, *Thermal Engng* **19**(9), 35–39 (1972).
20. N. S. Murty and V. M. K. Sastri, Direct contact heating of laminar falling liquid jets, *Int. J. Heat Mass Transfer* **19,** 115–117 (1976).
21. N. S. Mochalova, L. P. Kholpanov, V. A. Malyusov and N. M. Zhavoronkov, Heat transfer during condensation of vapor on a laminar jet of liquid with an initial segment, *J. Engng Phys.* **40,** 337–340 (1980).
22. J. Iciek, The hydrodynamics of a free liquid jet and their influence on direct contact heat transfer, *Int. J. Multiphase Flow* **9,** 167–179 (1983).
23. N. S. Mochalova, L. P. Kholpanov and V. A. Malyusov, Heat transfer in vapor condensation on laminar and turbulent liquid jets, taking account of the inlet section and variability of the flow rate over the jet cross section, *J. Engng Phys.* **54,** 486–489 (1988).
24. K. V. Dementyeva and A. M. Makarov, Condensation of vapor on free cold-liquid jets, *Heat Transfer—Sov. Res.* **6**(1), 116–119 (1974).
25. T. C. Hoang and R. A. Seban, The heating of a turbulent water jet discharged vertically into a steam environment, *Int. J. Heat Mass Transfer* **31,** 1199–1209 (1988).
26. S. S. Kutateladze, I. I. Gogonin and V. I. Sosunov, The influence of condensate flow rate on heat transfer in film condensation of stationary vapour on horizontal tube banks, *Int. J. Heat Mass Transfer* **28,** 1011–1018 (1985).
27. S. Kim and A. F. Mills, Condensation on coherent turbulent liquid jets, *ASME J. Heat Transfer* **111,** 1068–1082 (1989).
28. G. P. Celata, M. Cumo, G. E. Farello and G. Focardi, A comprehensive analysis of direct contact condensation of saturated steam on subcooled liquid jets, *Int. J. Heat Mass Transfer* **32,** 639–654 (1989).
29. V. P. Isachenko, S. A. Sotskov and E. V. Yakusheva, Heat transfer during condensation of water vapor on a laminar cylindrical water jet, *Thermal Engng* **23**(8), 60–62 (1976).
30. H. R. Jacobs and R. Nadig, Condensation on coolant jets and sheets including the effects of noncondensible gases, *ASME J. Heat Transfer* **109,** 1013–1020 (1987).
31. A. N. Reznikov and V. N. Gavrilov, An approximation of probability integral by elementary function, *J. Engng Phys.* **8,** 379–381 (1967) [in Russian].
32. D. Marsal, *Die numerische Lösung partieller Differentialgleichungen in Wissenschaft und Technik*. Bibliographisches Institut AG, Zürich (1976).
33. W. A. Stein, Neue Gleichungen für die Transportvorgänge bei überströmten Einzelkörpern (Teil 2), *Forsch. Ing Wes.* **56,** 133–148 (1990).
34. T. L. Lui, H. R. Jacobs and K. Chen, An experimental study of direct condensation on a fragmenting circular jet, *ASME J. Heat Transfer* **111,** 585–588 (1989).